SUPPORTING INFORMATION

Contents:

1. Experimental Methods and results

1.1 Materials

Three types of titania nanoparticles were considered. One was constituted by lab-made TiO_2 NPs, 100% anatase, prepared via hydrothermal synthesis, and then coded as TiO_2 HT, with a procedure similar to that developed by Sugimoto, but without the intermediate gelation step [1]. Details of preparation, structural and morphological characterization are in ref. 2. In summary, these NPs were obtained by forced hydrolysis of 40 mM aqueous solution of $Ti(TEOA)_2$ complex (TEOA = triethanolamine; initial pH 10), carried out by hydrothermal treatment at 453 K for 96 h). At the end of the hydrothermal treatment the sample was calcined at 673 K for 2 hours. The specific surface area, measured by adsorption of N_2 at 77 K and applying the BET model (SSA_{BET}), of the as prepared powder was of ca. 42 $m^2 \cdot g^{-1}$, and decreased slightly to ca. 37 $m^2 \cdot g^{-1}$ after outgassing/oxidation at 873 K in the IR cell (see below). A second type was P25 by Evonik (formerly Degussa), 80% anatase and 20% rutile. The SSA_{BET} of the received nanopowder was ca. 55 $m^2 \cdot g^{-1}$, that decreased to ca. 40 $m^2 \cdot g^{-1}$ when treated at 873 K. The third type was prepared by Solaronix (www.solaronix.com), and coded as SX001. The procedure, similar to that developed by Ito et al. [3], was based on the hydrolysis of titanium isopropoxide (Dorf Ketal Tyzor® TPT) in at 493 K for 18 h. The suspension of TiO_2 NPs resulting from the synthesis was concentrated using a rotavapor system and then processed according to the following procedure: i) dialysis against ultrapure water (MilliQ, Millipore) using a Spectra/Por dialysis membrane tubing (MWCO 8-12 kD or MWCO 12-14 kD); final pH of the permeated liquid in the 5-6 range, Cl^- and SO_4^{2-} < 1 ppm (by ion chromatography); the suspension becomes thixotropic; ii) freeze-drying; iii) resuspension in milli-Q water; iv) irradiation for 48 hours of the suspension in contact with air, added of 10 ml of H_2O_2 (30%), under UV light using a medium pressure mercury lamp (emission max at 360 nm), ca. 10 W/m^2 in the range 290-400 nm; followed by dialysis and free-drying as steps i) and ii). The obtained TiO_2 powder was 100% anatase (Figure S1) and exhibited a SSA_{BET} of 93 $m^2 \cdot g^{-1}$. After outgassing/oxidation at 873 K in the IR cell the crystal phase was retained (Figure S1), whereas the SSA_{BET} decreased to 43 $m^2 \cdot g^{-1}$.

For thermal treatments in the IR cell and spectroscopic measurements of adsorbed probe molecules high purity O_2 and CO (99.999%, Praxair) were used, respectively, without any further purification except liquid nitrogen trapping.

References

1. T. Sugimoto, X. P. Zhou, A. Muramatsu, *J. Colloid Interface Sci.* **2003**, *259*, 43–52.

2. C. Deiana, M. Minella, G. Tabacchi. V. Maurino, E. Fois, G.Martra, *Phys. Chem.Chem.Phys*. **2013**, *15*, 307-315.

3. S.Ito, T. N. Murakami, P. Comte, P. Liska, C. Grätzel, M. K. Nazeeruddin, M. Grätzel, *Thin Solid Films*, **2008**, *516*, 4613–4619.

1.2 XRD

X-ray diffraction (XRD) pattern of the powders were recorded with an Analytical X'Pert Pro equipped with an X'Celerator detector powder diffractometer using Cu K_α radiation generated at 40 kV and 40 mA. The instrument was configured with 1/2° divergence and receiving slits. A quartz sample holder was used. The 2θ range was from 20° to 80° with a step size (°2θ) of 0.05 and a counting time of 3 s.

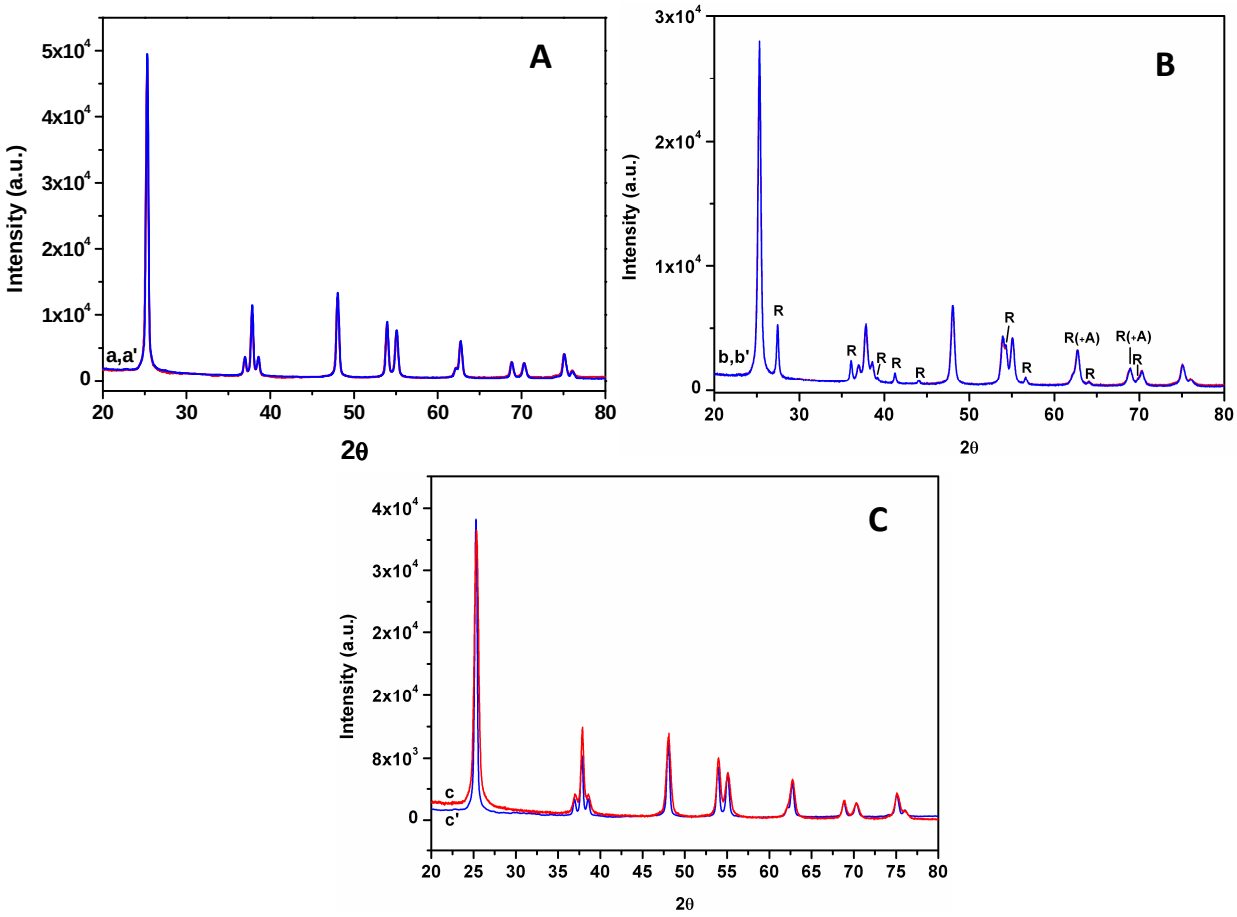

Figure S1. XRD patterns of TiO_2 HT (Panel A), TiO_2 P25 (Panel B) and TiO_2 SX001 (Panel C) as received (a, b, c red lines) and after the treatment at 873K, carried out before IR measurements of adsorbed CO (a',b',c' blue lines). Details on the treatment are in section 1.4.

Comment on Figure S1:

The XRD patterns reported in Figure S1 show the presence of the anatase phase only for the TiO_2 HT (panel A) and SX001 (panel C) samples, while, in the case of TiO_2 P25 (panel B; R= rutile; A= anatase), the presence of a mixture of anatase and rutile phases, typical for this material (~80% anatase, ~20% rutile) is observed. The XRD patterns collected before and after the activation at 873 K in the IR cell (see section 1.4) are almost identical in number, position and relative intensity, thus indicating that no anatase-rutile phase transition has occurred at that temperature. The only evolution observed in the case of TiO_2 SX001 is the narrowing of the diffraction peaks, in agreement with the more significant decrease of specific surface area observed for this material, with respect to the other two (see section 1.1. Materials)

1.3 TEM

TEM images were obtained with a Jeol 3010 instrument, operated at 300 kV. For the observation, powders were contacted in dry form with standard Cu grids coated with a lacey carbon film, and then introduced in the microscope.

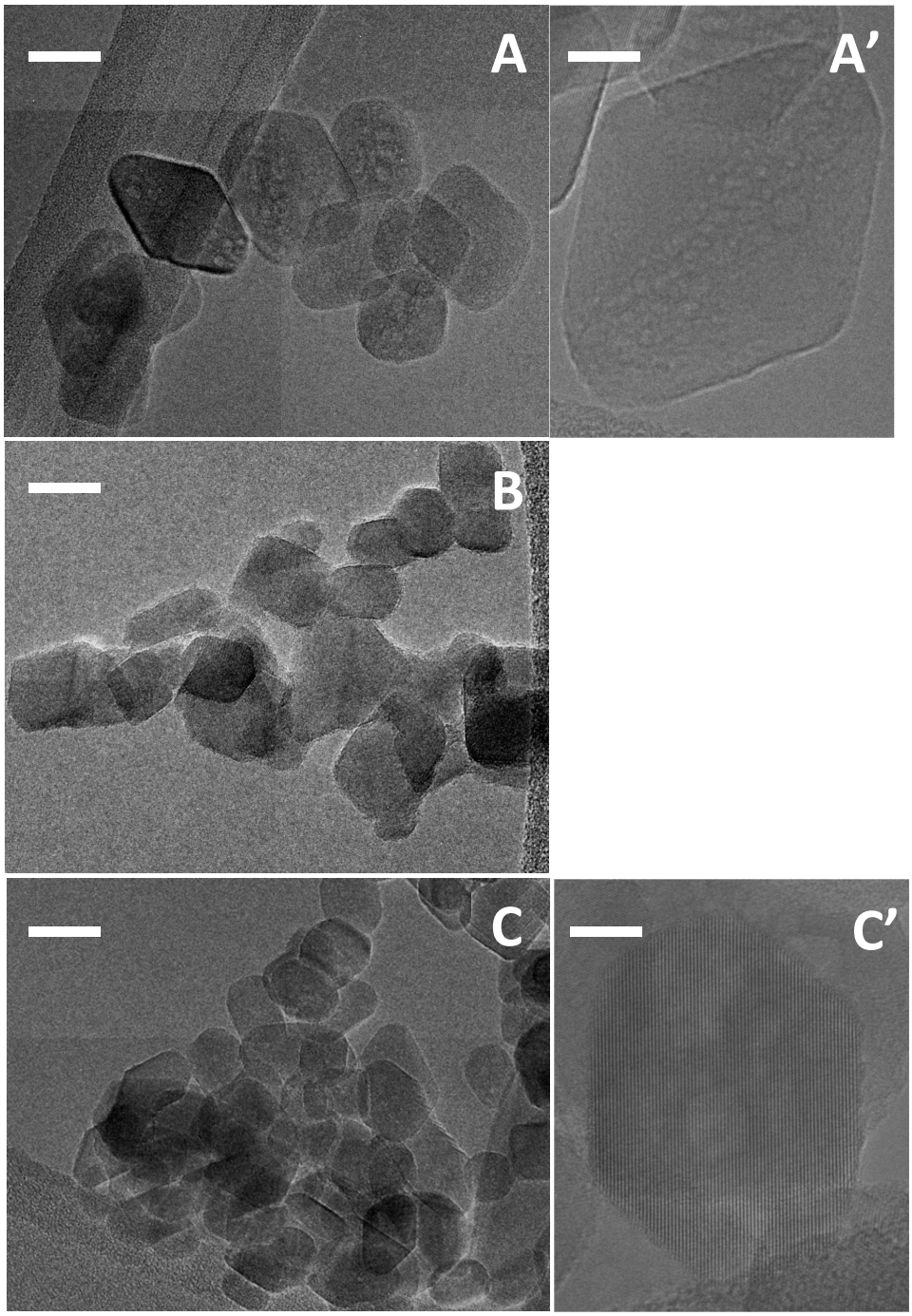

Figure S2. Representative TEM images of TiO_2 nanoparticles of the HT (A), P25 (B) and SX001 (C) types, after the treatment at 873 K carried out before IR measurements of adsorbed CO. Details on the treatment are in section 1.4. Original magnification 120k ×. Scale bar in panels A,B,C= 20 nm; scale bar in panels A', C'= 5 nm

Next page: comment on the figure

Comment on Figure S2:

TiO_2 nanoparticles exhibit more regular shape and borders in the case of TiO_2 HT (panel A), whereas for TIO_2 P25 and SX001 (panels B and C, respectively) are characterized by less regular profiles, in agreement with the presence of a significant fraction of surface terminations different from {101} facets (the most stable), as probed by IR spectroscopy of adsorbed CO (see main text, Figure 2 and related comments and Figure S4 below). Details on the interpretation of TEM images of TiO_2 nanoparticles, in particular on the effect of the projection on the 2D image plane of the shape of 3D object are in ref. 1.

Panels A' and C' are images at higher magnification of single TiO_2 HT (panel A') and TiO_2 SX001 (panel C') nanoparticles, showing the presence of inhomogeneity in the mass/thickness contrast, ascribed to the presence of inner voids. [1]

Reference

(1) C. Deiana, M. Minnella, G. Tabacchi, V. Maurino, E. Fois, G. Martra, *Phys. Chem. Chem. Phys.* **2013,** *15*, 307-315.

1.4 IR spectroscopy

Method

The powders were pressed in self-supporting pellets, with 10-15 mg/cm^2 as "optical thickness", and then inserted in a quartz cell with KBr windows, designed to carry out IR measurements at ca. 100 K, by cooling down with liquid nitrogen. The cell was connected to a conventional vacuum line (residual pressure ≤ 1 × 10^{-5} mbar) allowing the thermal treatment and the adsorption-desorption measurements to be carried out *in situ*. The samples were activated before IR measurements by thermal treatment at 873 K in presence of O_2 (6 mbar) for 60 min, then the pellets were cooled down to 473 K still in contact with oxygen, and further cooled down to room temperature under outgassing. At the end of the procedure the samples were white in color, as expected for fully oxidized TiO_2. The IR measurements were performed with a Bruker IFS28 equipped with a MCT detector, and with resolution of 2 cm^{-1}. The spectra of adsorbed CO were collected in Absorbance, after subtraction of the spectra obtained before CO admission.

Results

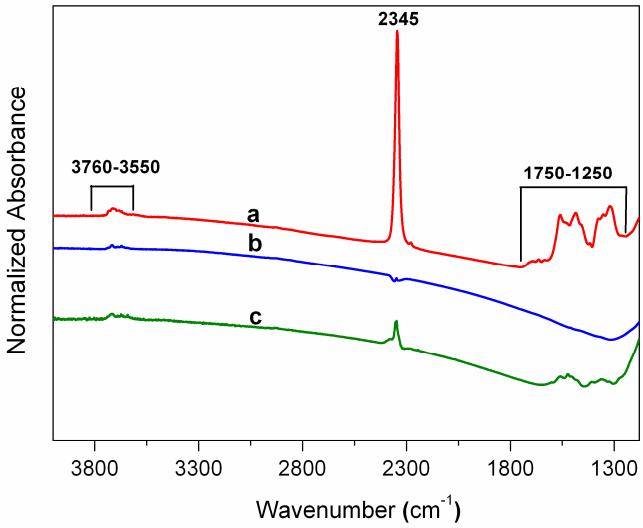

Figure S3. IR spectra of (a) TiO_2 HT, (b) TiO_2 P25 and (c) TiO_2 SX001 treated at 873 K as indicated in the IR experimental paragraph above. Spectra were normalised with respect to the mass of the pellets ("optical thickness", mg·mm^2) and SSA_{BET} of the material after thermal treatment.

Comment on Figure S3

After the treatment at 873 K, only very weak signals at 3760-3550 cm^{-1} due to the few OH groups which resisted outgassing were observed for all samples. In addition, for TiO_2 HT and SX001 additional bands were present: an intense peak at 2345 cm^{-1}, due to the antisymmetric stretching mode of slightly perturbed CO_2 and a complex pattern in the 1750-1250 cm^{-1} range, typical of carboxylates/carbonates groups. The resistance of these species, resulting from the oxidation of organic moieties used for the synthesis, to the thermal treatment indicates that they should be entrapped in/at the inner surface of voids present in these materials (see TEM images above).

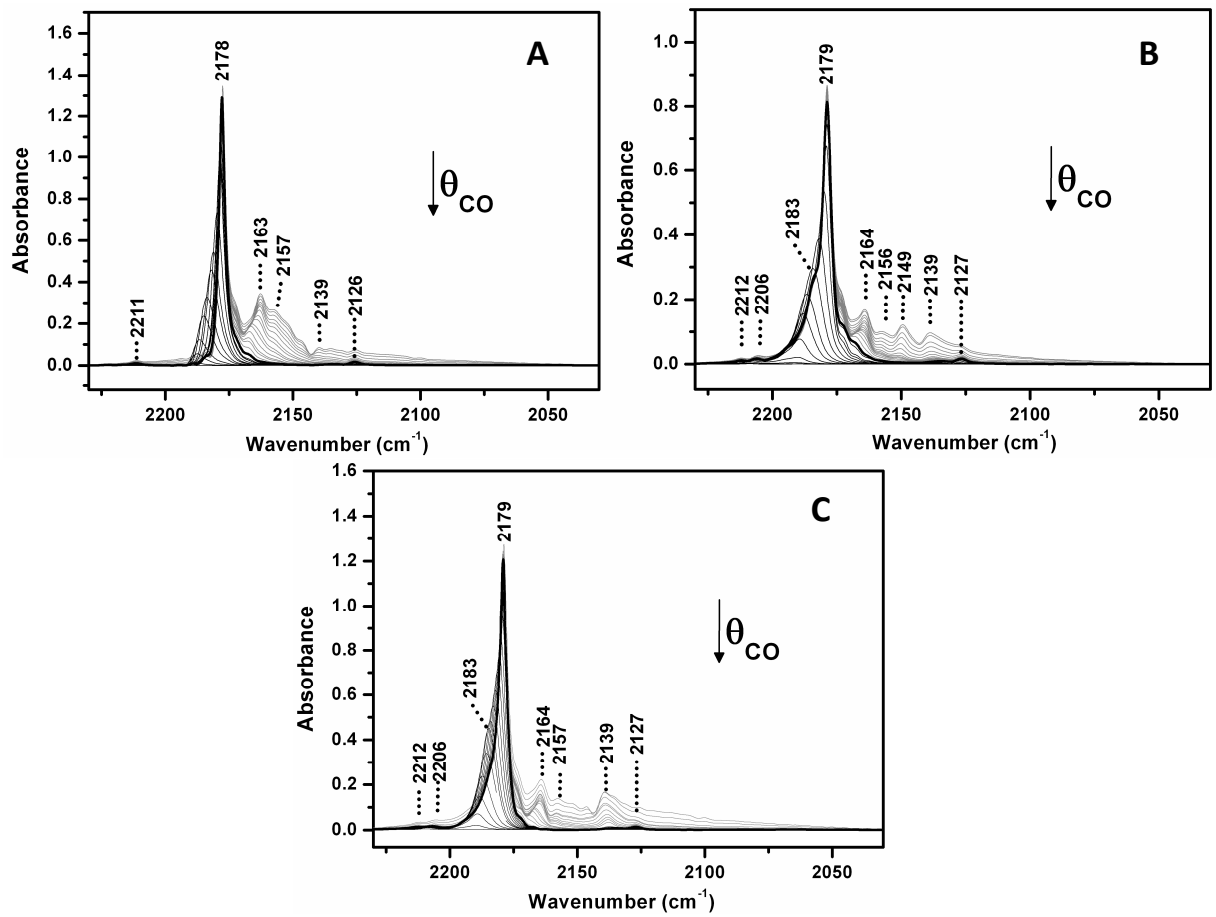

Figure S4. IR spectra of CO adsorbed at ca. 100 K on (A) TiO_2 HT, (B) TiO_2 P25 and (C) TiO_2 SX001 outgassed at 873 K (details in the IR experimental section above). Spectra were collected at decreasing coverages (θ_{CO}), from 60 mbar CO to outgassing for 10 min at ca. 100 K. Panels A and B adapted from the Supporting Information of ref.[1]

Comment on Figure S4:

Spectral components between the weak components at 2206 cm^{-1} (present for CO on TiO_2 P25, panel B, and on TiO_2 SX001, panel C) and 2127/2126 cm^{-1} are due to the internal stretching mode of CO molecules adsorbed on surface sites different in local structure or nature. On the basis of ref. 1 and where specified of ref. 2, they can be assigned to:

- 2206 cm^{-1}: CO on Ti^{4+} surface ions corresponding to the so called "α sites"
- 2183 cm^{-1}: CO on Ti^{4+} sites at {110} surface facets
- 2179/2178 cm^{-1}: CO on Ti^{4+} sites at {101} surface facets

These carbonylic adducts are more resistant to the decrease of CO coverage than those at lower frequency as results from the comparison between grey and black curves in the three panels. Thus, for the sake of simplicity, only black curves were considered for the figure in the main text showing the effect of the decrease of CO coverage on the 2183 and 2179/2178 cm^{-1} signals.

- 2164/2163 cm^{-1}: CO on Ti^{4+} sites at {100} and/or {001} surface facets
- 2157/2156 cm^{-1}: CO on surface OH which resisted the outgassing at 873 K
- 2149 cm^{-1}: CO on Ti^{4+} exposed at the surface of rutile nanoparticles in TiO_2 P25
- 2139 cm^{-1}: CO physisorbed in liquid-like multilayers
- 2127/2126 cm^{-1}: ^{13}CO (natural abundance) on Ti^{4+} sites at {101} surface facets

(continue)

In addition, as reported in ref. 3 the weak signal at 2212/2211 cm^{-1} is due to the combination mode between the internal stretching and frustrated translational modes of CO on Ti^{4+} sites at {101} surface facets.

References

(1) C. Deiana, M. Minnella, G. Tabacchi, V. Maurino, E. Fois, G. Martra, *Phys. Chem. Chem. Phys.* **2013,** *15*, 307-315.

(2) L. Mino, A. M. Ferrari, V. Lacivita, G. Spoto, S. Bordiga and A. Zecchina, *J. Phys. Chem. C* **2011**, *115*, 7694-7700.

(3) C. Deiana, G.Tabacchi, V. Maurino, S. Coluccia, G. Martra, E. Fois, *Phys. Chem. Chem. Phys.* **2013**, *15*, 13391–13399.

2. Modeling

2.1 Computational methods

The adsorption of carbon monoxide on TiO_2 in the low-coverage regime ($\theta \rightarrow 0$) was simulated by using periodic slab models of anatase TiO_2 surfaces, which had already been extensively tested and successfully adopted to elucidate CO adsorption on different types of TiO_2 facets at the full-coverage regime ($\theta \rightarrow 1$).[1,2] In particular, for the present work we adopted:

i) a slab model of the TiO_2 anatase (101) surfaces, which expose pentacoordinated Ti sites and are predominant in all the three types of TiO_2 nanoparticles adopted in the IR experiments, namely HT, SX001 and P25;
ii) a slab model of the TiO_2 anatase (110) surfaces, which are characterized by tetracoordinated Ti sites and represent an appreciable portion of the exposed surfaces in the P25 (considering the anatase prevailing fraction) and SX001 nanoparticles.

The content of the simulation cell for the TiO_2 (101) surface model is $6(Ti_6O_{12})$ while that of the TiO_2 (110) surface model is $8(Ti_4O_8)$. The in-plane dimensions (x,y) of the simulation cell are $(10.239 \times 11.355)Å^2$ for the TiO_2(101) surface and $(10.706 \times 9.514)Å^2$ for the TiO_2(110) one. Both surface models, represented in Figure S5, are stoichiometric and exhibit regular facets.

Electronic structure calculations were performed within the density functional theory (DFT) framework; in particular, electronic interactions were approximated with the Perdew-Burke-Ernzerhof (PBE) formulation of DFT.[3] Plane waves (PW) were adopted as basis set: specifically, a cutoff of 80 Ry was used for the electronic states, while a cutoff of 320 Ry was adopted for the electron density representation. The electron-ionic core interactions were described by adopting norm-conserving pseudopotentials[4] for all atoms; in the case of Ti, a full core norm-conserving pseudopotential (i.e. a Ti^{4+} is considered) was used, along with the Non Linear Core Correction scheme.[5] With this pseudopotential choice, structural, vibrational and electronic properties of a variety of Ti-containing systems were properly reproduced; [6-11] moreover, a proper description of CO adsorption on various types of TiO_2 anatase facets at the full-coverage regime was obtained.[1,2] Periodic boundary conditions were adopted in three dimensions. A vacuum region of 1.2 nm along the z direction was adopted to alleviate inter-slab interactions.

Only the Γ point of the Brillouin zone was used. The convergence of geometrical parameters with respect to both cutoff and Brillouin zone sampling had been validated previously (see Ref. 1 for further details). Geometry optimizations were carried out with a quasi-Newton approach by adopting a convergence criterion of a maximum force of 1×10^{-4} hartree/bohr. All atoms were allowed to relax with the exception of the lowest layer ones, which were fixed at the experimental coordinates from diffraction data.

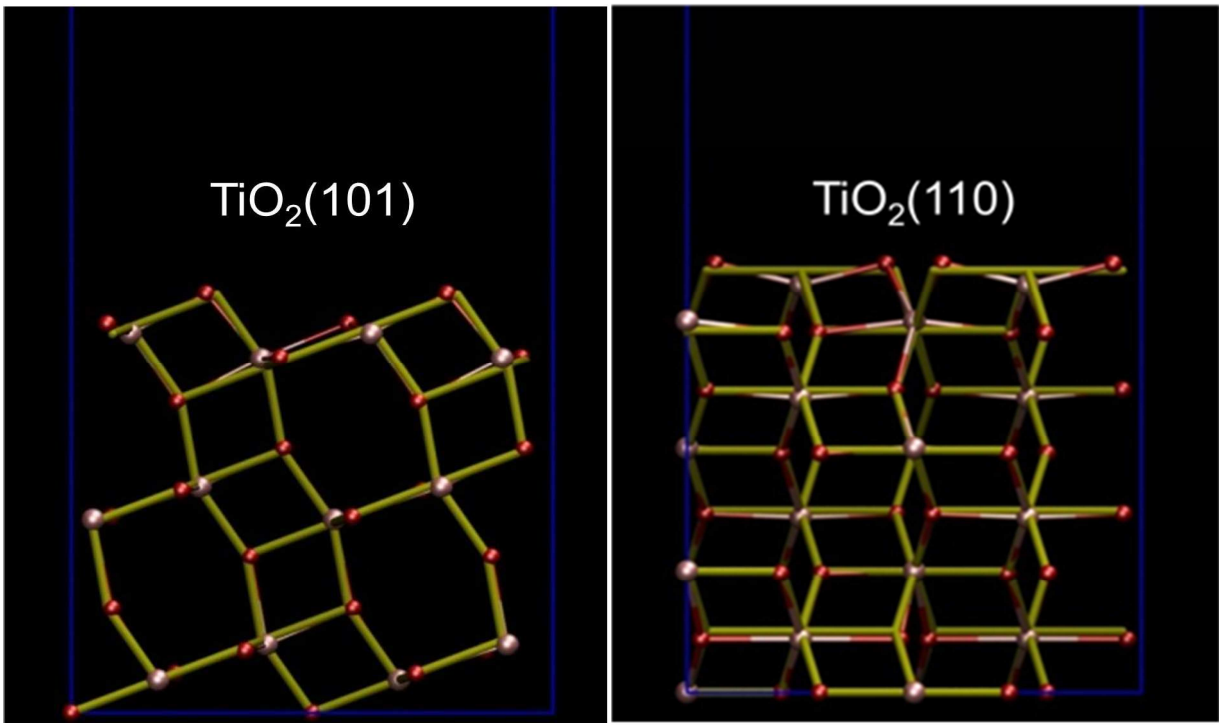

Figure S5. Side-view (xz-plane) of the TiO_2 anatase slabs adopted for the calculations. The blue line indicates the periodicity. The yellow sticks represent the structure of the unrelaxed TiO_2 slabs. The relaxed (optimized) structures are represented in ball-and-stick. Red spheres represent oxygen atoms, pink spheres represent Ti atoms. Interestingly, upon relaxation of the slab, the top layer is particularly affected: under-coordinated Ti atoms are pushed slightly inside the surface, while oxygen atoms are pushed outward.

To study carbon monoxide absorption at the low-coverage regime, we considered the optimized TiO_2 (101) and TiO_2(110) surface models and positioned one CO molecule on the top of each slab. The geometry of the two surface-molecule systems was then optimized, leading to the CO@TiO_2(101) and CO@TiO_2(110) structures discussed in this work and shown in Figure 1 of the main text.

The electronic structure analysis was performed on the optimized geometries by projecting the Kohn-Sham orbitals on atomic functions. The most relevant results are discussed in the main text, while further data, as well as additional contour plots of the electronic valence states of the CO-TiO_2 systems most localized on CO are shown in the following Section 2.2.

Vibrational harmonic frequencies were calculated numerically via a finite difference approach. The results of these calculations confirmed that the CO@TiO_2(101) and CO@TiO_2(110) structures actually correspond to minima of the potential energy surface, characterized by positive vibrational frequencies. The reliability of this computational approach in reproducing the experimentally observed relative shifts of the CO stretching mode on different types of TiO_2 surfaces has already been demonstrated in Refs. 1 and 2, where the calculated values were scaled to facilitate comparison with experimental data. In the present work, the same scaling factor (1.011754)[1] was applied to the calculated vCO wavenumbers. The resulting values obtained for the CO@TiO_2(101) and CO@TiO_2(110) models are reported in Table 1 of the main text.

The surface-molecule interactions were also investigated by evaluating the CO-surface binding energy and by comparing the structural, vibrational, and electronic properties of the adsorbed CO molecule with the corresponding quantities calculated for the isolated CO molecule. Such reference data were obtained by optimizing the structure of a CO molecule in the same simulation cell adopted for each CO-TiO_2 model

and then calculating the corresponding vibrational and electronic properties. However, no significant difference was found among the values calculated with the two simulation cells.

The CO-surface binding energies were calculated on the optimized structures using the formula:

$$-BE = E([TiO_2]_n\text{-}CO) - E([TiO_2]_n) - E(CO),$$

where $E([TiO_2]_n\text{-}CO)$ is the energy of the optimized slab with one CO adsorbed molecule, $E([TiO_2]_n)$ is the energy of the optimized slab and E(CO) is the energy of the CO molecule calculated in the corresponding simulation cell (n=36 for $CO@TiO_2(101)$ and n=32 for $CO@TiO_2(110)$). The calculated binding energies (in kJ mol^{-1}) are reported in Table 1 in the main text.

The CPMD code was adopted for all the calculations performed in this work.[12]

References

[1] C. Deiana, M. Minella, G. Tabacchi, V. Maurino, E. Fois, G. Martra, *Phys. Chem. Chem. Phys.* **2013**, *15*, 307-315

[2] C. Deiana, G.Tabacchi, V. Maurino, S. Coluccia, G. Martra, E. Fois, *Phys. Chem. Chem. Phys.* **2013**, *15*, 13391–13399.

[3] J. P. Perdew, K. Burke, M. Ernzerhof, *Phys. Rev. Lett.* **1996**, *77*, 3865-3868.

[4] N. Troullier, J. L. Martins, *Phys. Rev. B* **1991**, *43*, 1993-2006.

[5] S. G. Louie, S. Froyen, M. L. Cohen, *Phys. Rev. B* **1982**, *26*, 1738-1742.

[6] E. Fois, A. Gamba, E. Spano, *J. Phys. Chem. B* **2004**, *108*, 154-159.

[7] E. Fois, A. Gamba, G. Tabacchi, *ChemPhysChem* **2005**, *6*, 1237-1239.

[8] E. Fois, A. Gamba, G. Tabacchi, *ChemPhysChem* **2008**, *9*, 538-543.

[9] A. Gamba, G. Tabacchi, E. Fois, *J. Phys. Chem. A* **2009**, *113*, 15006-15015.

[10] E. Spano, G. Tabacchi, A. Gamba, E. Fois, *J. Phys. Chem. B* **2006**, *110*, 21651-21661.

[11] G. Tabacchi, E. Gianotti, E. Fois, G. Martra, L. Marchese, S. Coluccia, A. Gamba, *J. Phys. Chem. C* **2007**, *111*, 4946-4955.

[12] CPMD: Car–Parrinello Molecular Dynamics, Version 3.17.1, IBM Corp. **1990–2015** and MPI für Festkörperforschung Stuttgart **1997–2001** (www.cpmd.org)

2.2. Analysis of the electronic structure of CO@TiO_2(101) and CO@TiO_2(110)

2.2.1 Electronic density of states

Figure S6 shows the total density of electronic states (DOS) calculated for the CO@TiO_2(101) and CO@TiO_2(110) systems, as well as the projected density of states on the Ti atoms, on the surface oxygen atoms, and on the carbon monoxide atoms. The latter one (shown as a blue line in Figure S6) is also displayed in Figure S7 (adapted from Figure 3 and the bottom part of Figure 5 of the main text) for the sake of clarity.

Figure S6 shows that, for both CO@TiO_2(101) and CO@TiO2(110) systems, the prominent part of the total DOS at high energies is composed, as expected, by p-states of the oxygen atoms of the surface. The CO states contribute to the total DOS mainly below- 9.0 eV. For both systems, however, a small contribution of the CO states is present at higher energies. Because only main points of this aspects were discussed in the main text, additional comments are reported in this section, with the support of Figure S7.

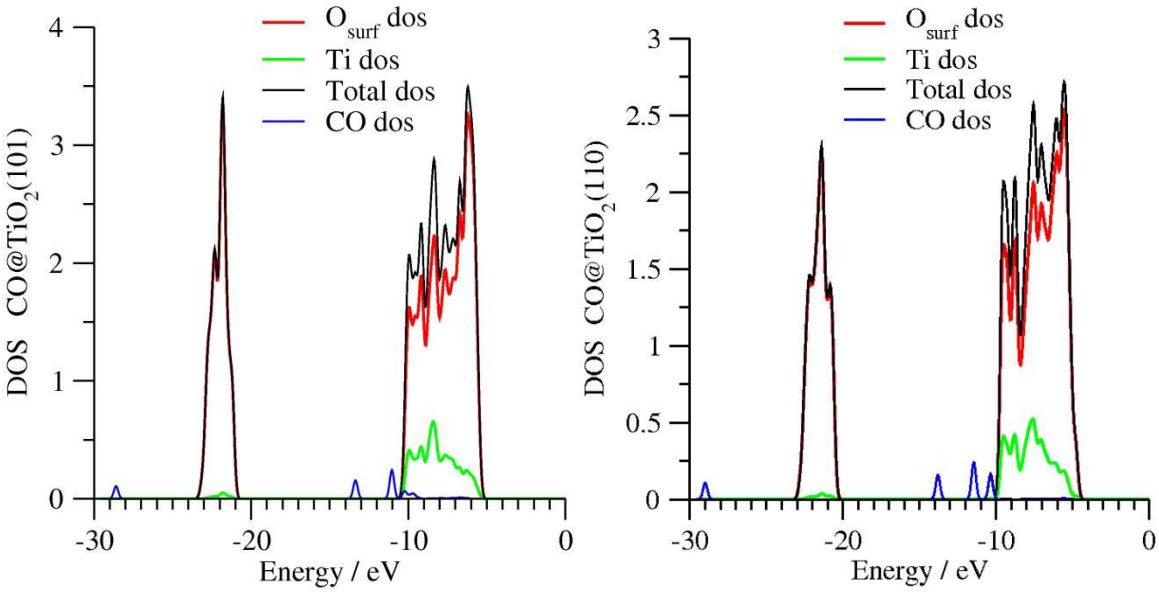

Figure S6. Total density of states (black) and density of states projected on the surface oxygen atoms O_{surf} (red); on Ti atoms (green); on carbon monoxide (blue), calculated for the CO@TiO_2(101) and CO@TiO_2(110) systems.

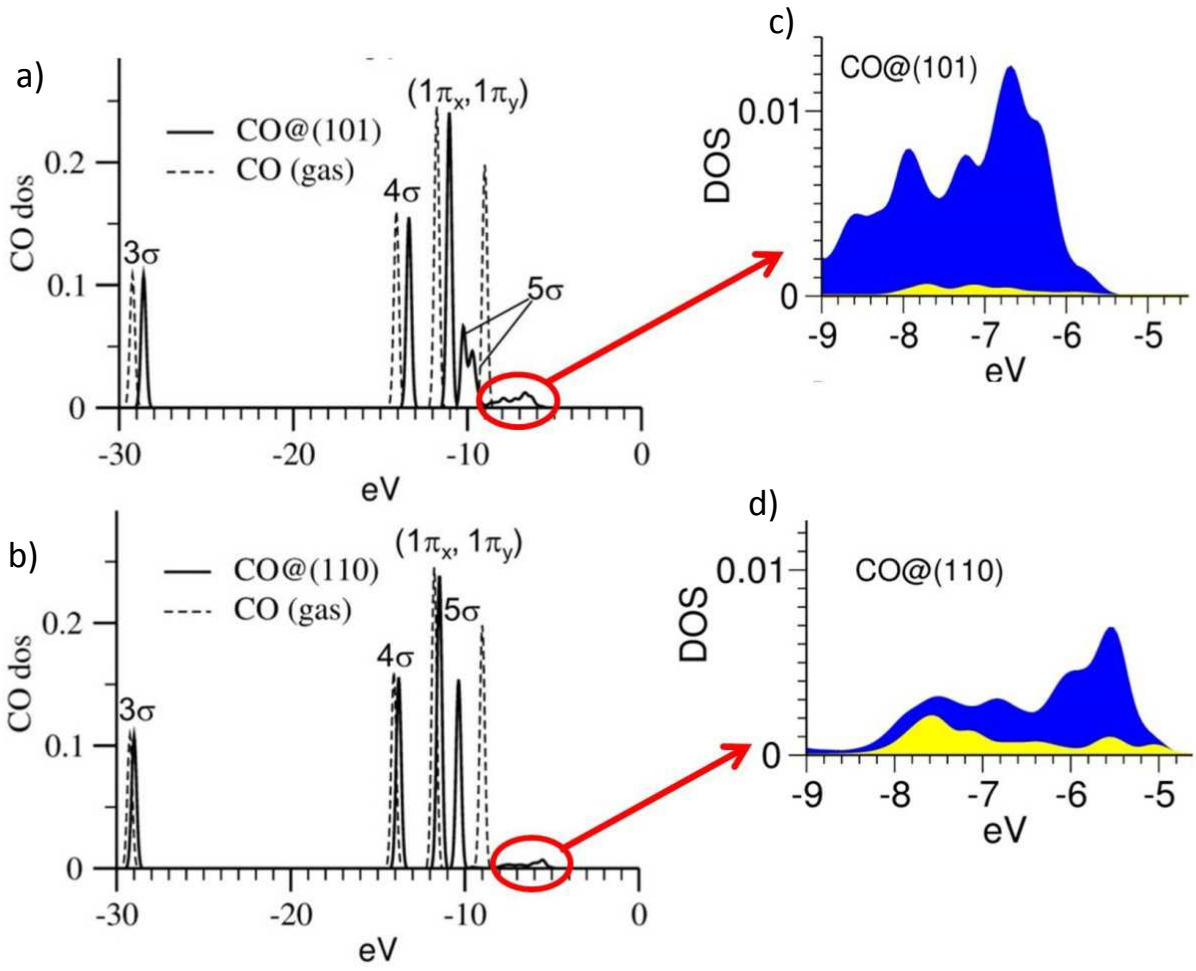

Figure S7. Left and right panels are adapted from Figure 3 and 5 of the main text, respectively.

Data in panels a) and b) indicate that the 3σ, 4σ, and the ($1\pi_x$, $1\pi_y$) orbitals of CO are slightly destabilized upon adsorption. Accordingly, the electronic states of the CO@TiO_2(110) and CO@TiO_2(110) systems reminiscent of these orbitals (shown in Figures S8, S9, S10, respectively), indicate that these valence orbitals of CO are only slightly perturbed upon adsorption to the surface, and that they do not play a major role in the surface-CO interaction.

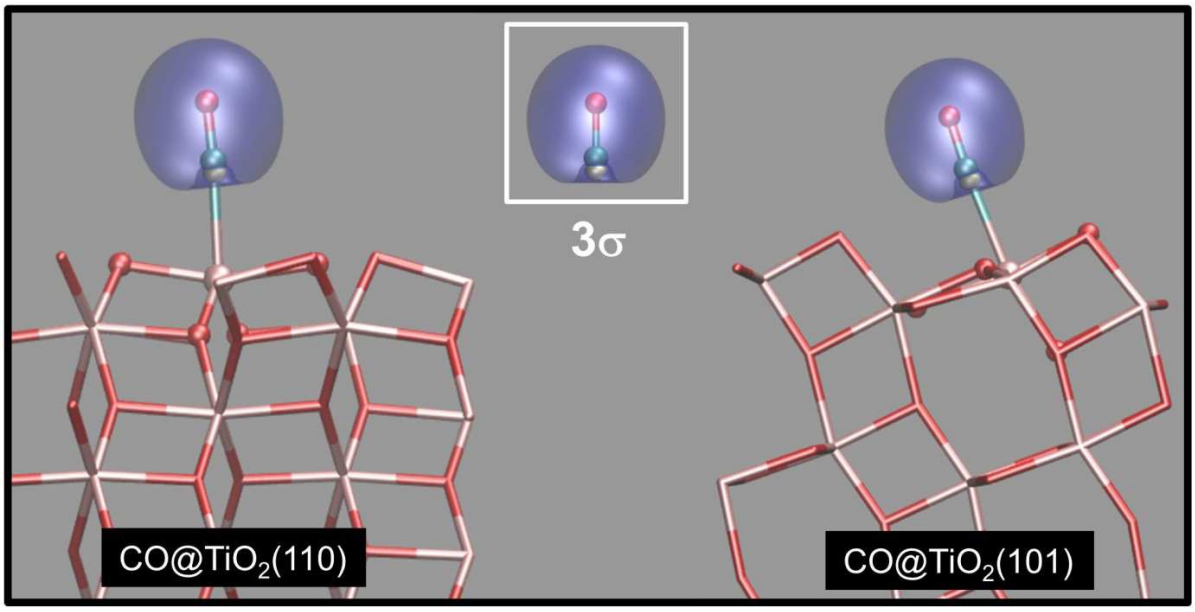

Figure S8. The electronic valence states of the molecule-surface systems (xz-projections) identifiable with the 3σ orbital of the isolated CO molecule. Atom colors: C=cyan, O=red, Ti=pink. Positive lobes: blue, negative ones: yellow.

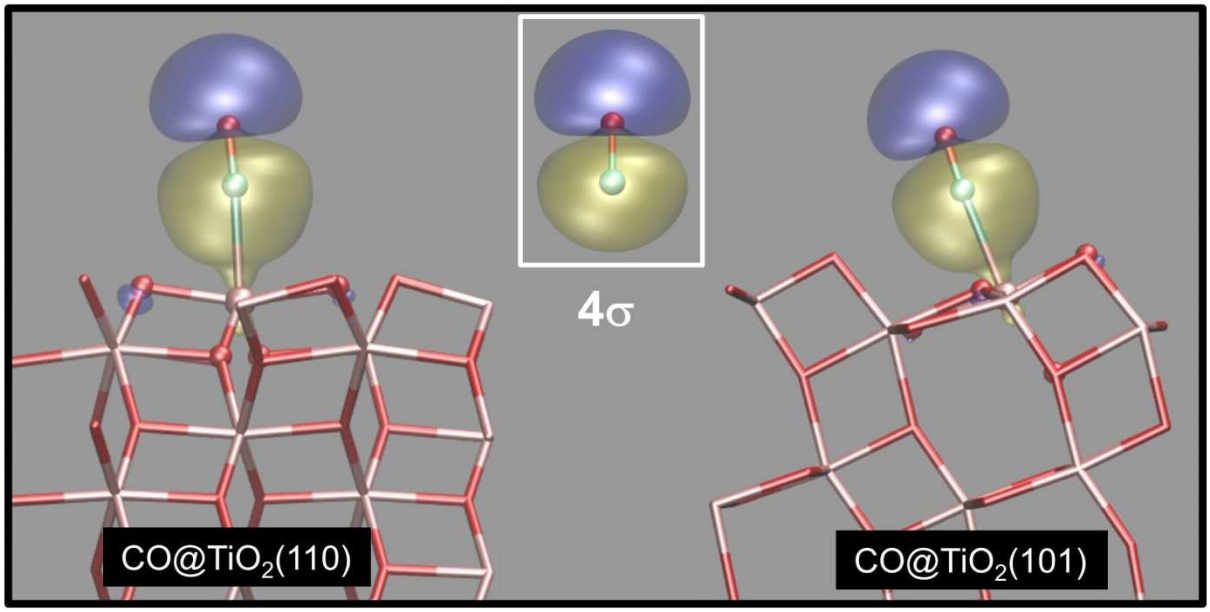

Figure S9. The electronic valence states of the molecule-surface systems (xz-projections) identifiable with the 4σ orbital of the isolated CO molecule. Atom colors: C=cyan, O=red, Ti=pink. Positive lobes: blue, negative lobes: yellow.

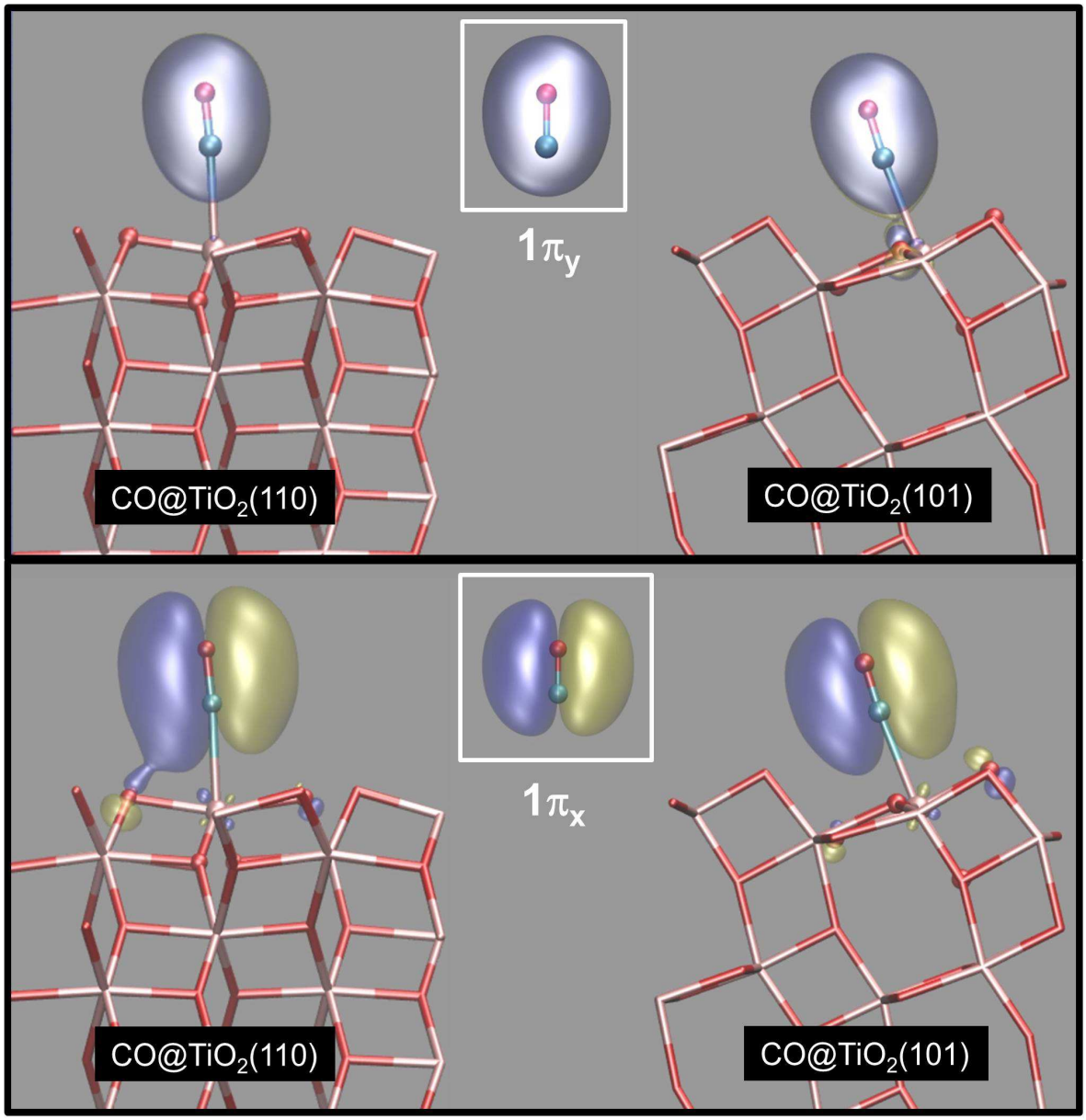

Figure S10. The valence states of the molecule-surface systems (xz-projections) identifiable with the $1\pi_x$ (bottom) and $1\pi_y$ (top) orbitals of the isolated CO molecule. Atom colors: C=cyan, O=red, Ti=pink. Positive lobes in blue, negative ones in yellow.

The stabilization of the 5σ orbital of CO upon adsorption and its role in the surface-molecule interaction are discussed in the main text. The electronic states of the $CO@TiO_2(110)$ and $CO@TiO_2(101)$ systems containing the maximum contribution of the 5σ state of CO are shown in Figure 3 of the main text. Figure S11 provides additional views of the same electronic states in order to further highlight the more localized nature of σ-bonding for $CO@TiO_2(110)$ compared to $CO@TiO_2(101)$.

As discussed in the main text, in the case of $CO@TiO_2(101)$, the contribution of the 5σ state to the CO DOS is split into two main peaks: the largest one corresponds to the state reported in Figures 3 in the main text and S11. Figure S12 shows the electronic state of the $CO@TiO_2(101)$ system corresponding to the smaller peak, which further illustrates the extensive mixing of the 5σ orbital of CO with the $TiO_2(101)$ valence band states and also highlights a σ-donation significantly more delocalized with respect to $CO@TiO_2(110)$.

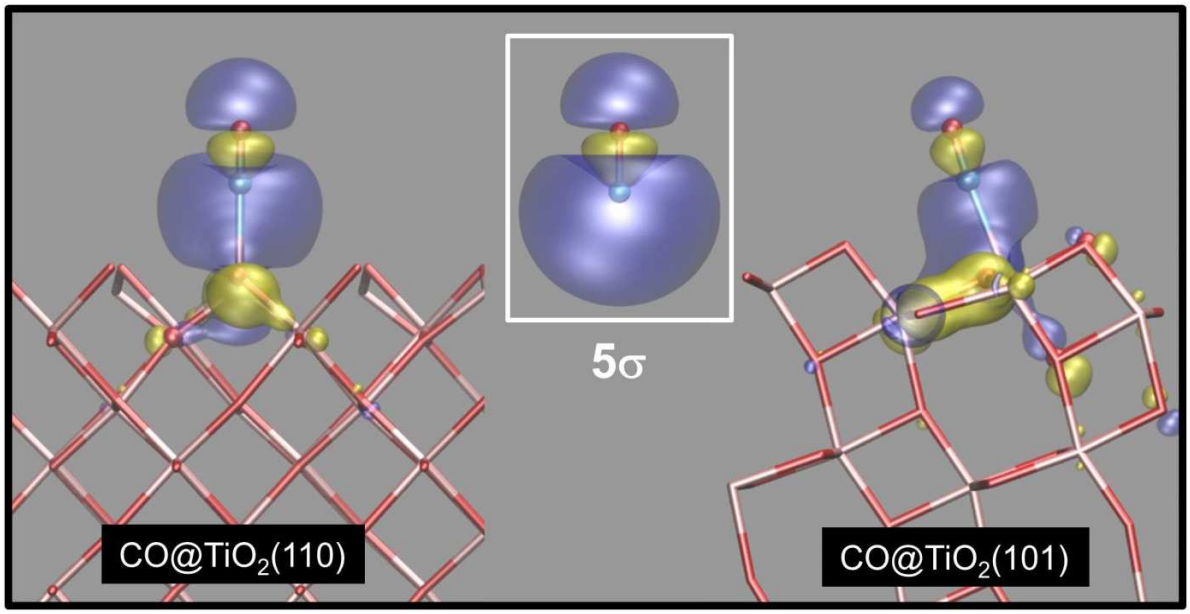

Figure S11. The electronic valence states of the molecule-surface systems with the highest contribution from the 5σ orbital of the isolated CO molecule (left panel: yz-projection, right panel: xz-projection). Atom colors: C=cyan, O=red, Ti=pink. Positive lobes in blue, negative ones in yellow.

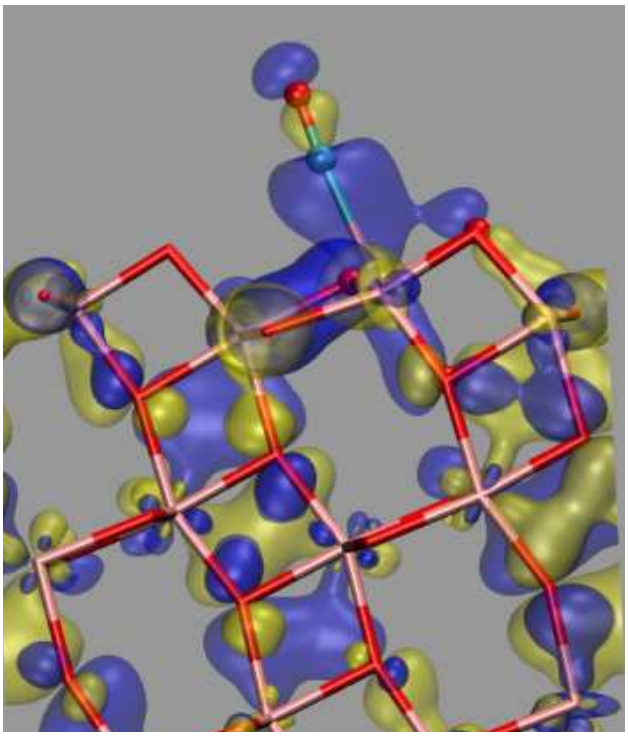

Figure S12: The electronic valence state of the CO@TiO_2(101) system (xz-projection) corresponding to the smaller component of the 5σ-peak of the CO DOS (see Figure 3a, main text). Atom colors: C=cyan, O=red, Ti=pink. Positive lobes in blue, negative ones in yellow.

Both the CO@TiO_2(101) and CO@TiO_2(110) systems show a small feature in their CO DOS at high energies (i.e., for *E* > -9 eV) (see the enlarged view of this feature in Figure S7 c) and d), blue areas). As discussed in the main text, a substantial contribution to this feature in the CO@TiO_2(110) case is given by states characterized by antibonding character with respect to the C-O bond. Some of these states are reminiscent of the $2\pi_x$* and $2\pi_y$* orbitals of gas phase CO, see, e.g. the orbitals shown in Figure 5c,d of the main text, while other ones feature a combination of the $2\pi_x$* and $2\pi_y$* states, like, e.g., the electronic state depicted in Figure S13. In order to estimate the total contribution of the $2\pi_x$* and $2\pi_y$* orbitals of carbon monoxide to the CO DOS of CO@TiO_2(101) and CO@TiO_2(110), we selected, among the electronic valence states of each system, all the ones characterized by lobes with opposite sign on the C and O atoms of carbon monoxide, and by antibonding character with respect to the C-O bond; the states collected in this way were then projected on the CO atoms. For CO@TiO_2(101) and CO@TiO_2(110), the resulting total 2π* contribution to the CO DOS is highlighted in yellow in Figure S7 c) and d), respectively.

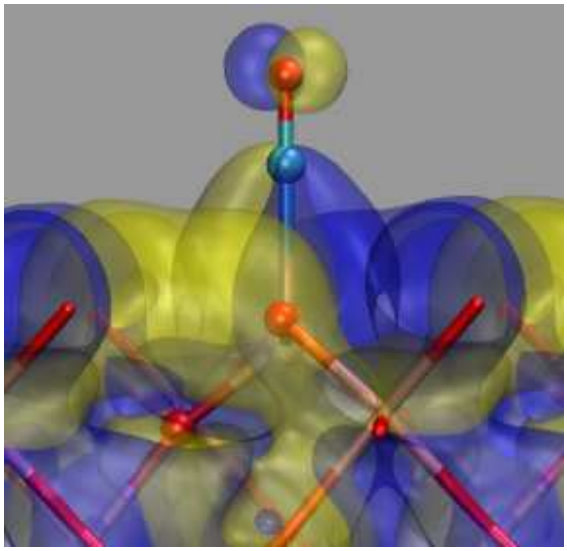

Figure S13. An electronic valence state of the CO@TiO_2(110) system (projected on the yz-plane) which contains contributions (on the C and O atoms) deriving from both the $2\pi_x$* and $2\pi_y$* states of gas phase CO. Atom colors: C=cyan, O=red, Ti=pink. Positive lobes in blue, negative lobes in yellow.

To the high energy feature of the CO DOS also contribute combinations of the CO 5σ orbital with the TiO_2 electronic states characterized by antibonding character with respect to the Ti-C bond. Whereas such states dominate the high-energy feature of the CO DOS in the (101) case (Figure S7,d), their contribution is less important in the CO@TiO_2(110) system. This can be understood by considering that the mixing of 5σ with the TiO_2 valence states is much more pronounced in the CO@TiO_2(101) case compared to CO@TiO_2(110). Two examples of these states are illustrated in Figure S14. Specifically, this Figure shows the orbitals of the CO@TiO_2(110) (left panel) and CO@TiO_2(101) (right panel) systems which have the highest contribution of the CO 5σ orbital and are antibonding with respect to the Ti-C bond. These states may be considered as the antibonding counterparts of the surface-CO orbitals responsible of σ-bonding shown in Figure 3 of the main text and in Figure S11.

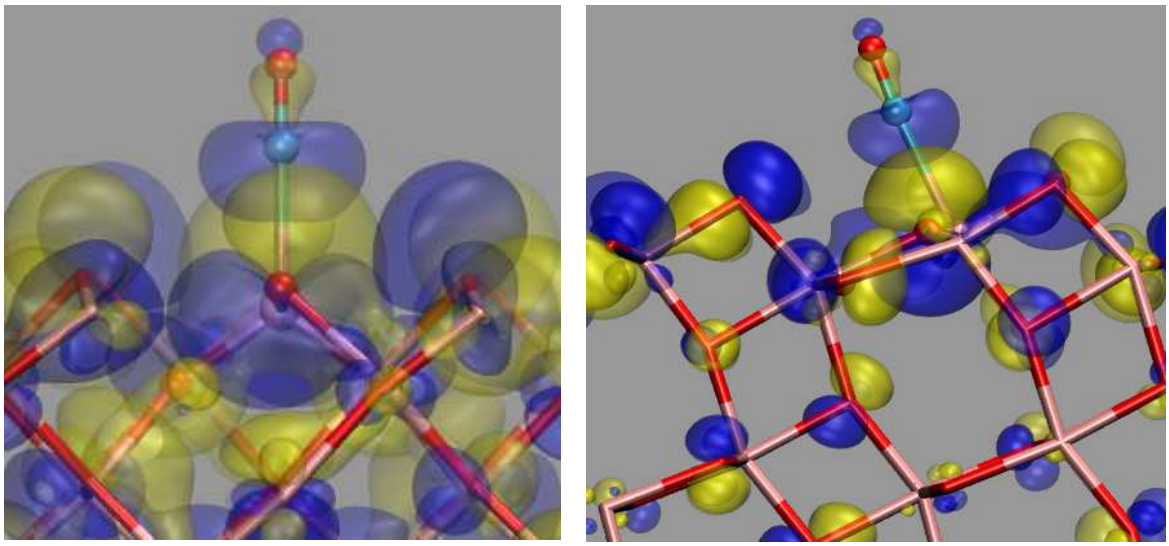

Figure S14. The valence states of the CO@TiO_2(110) system (left panel, yz-projection) and CO@TiO_2(101) system (right panel, xz-projection) characterized by the greatest contribution from the CO 5σ orbital and antibonding character with respect to the Ti-C bond. Atom colors: C=cyan, O=red, Ti=pink. Positive lobes in blue, negative ones in yellow.

2.2.2 Bonding charge density

The bonding charge density Δρ (also known as differential charge density or charge density difference) for a given system AB is defined (see, e.g. the reference of this subsection) as the difference between the electronic density of the system ρ(AB), and the sum of the electronic densities of the isolated subsystems (ρ(A)+ ρ(B)), i.e.,:

$$\Delta\rho(AB)= \rho(AB)- (\rho(A)+ \rho(B)).$$

For each isolated subsystem, the density is calculated on a geometry identical to that exhibited by the subsystem in the full system AB. Bonding charge density plots are particularly useful to visualize the effect of the interactions between subsystems on the electronic charge distribution.

Specifically, the bonding charge densities of the CO@TiO_2(110) and CO@TiO_2(101) systems were calculated using the optimized geometries of the full systems and the formulas:

$$\Delta\rho(CO@TiO_2\ (110)) = \rho\ (CO@TiO_2\ (110)) - [\rho\ (TiO_2\ (110)) + \rho\ (CO)]$$
$$\Delta\rho(CO@TiO_2\ (101)) = \rho\ (CO@TiO_2\ (101)) - [\rho\ (TiO_2\ (101)) + \rho\ (CO)]$$

In both cases, Δρ represents the change in electronic charge upon bringing the carbon monoxide molecule and the surface together. It is generally represented as an isosurface plot (see Figure 4 in the main text), or as a contour plot if a more quantitative estimation of the changes in the charge density is desired.

Contour plot representations of the bonding charge density of the CO@TiO_2(110) and CO@TiO(101) systems are depicted in Figure S15. This figure evidences that the accumulation of charge density between the Ti and C atoms (i.e. along the Ti-CO bond, which is not shown for clarity), as well as around the oxygen atom of CO, are significantly greater for CO@TiO_2(110) compared to CO@TiO_2(101).

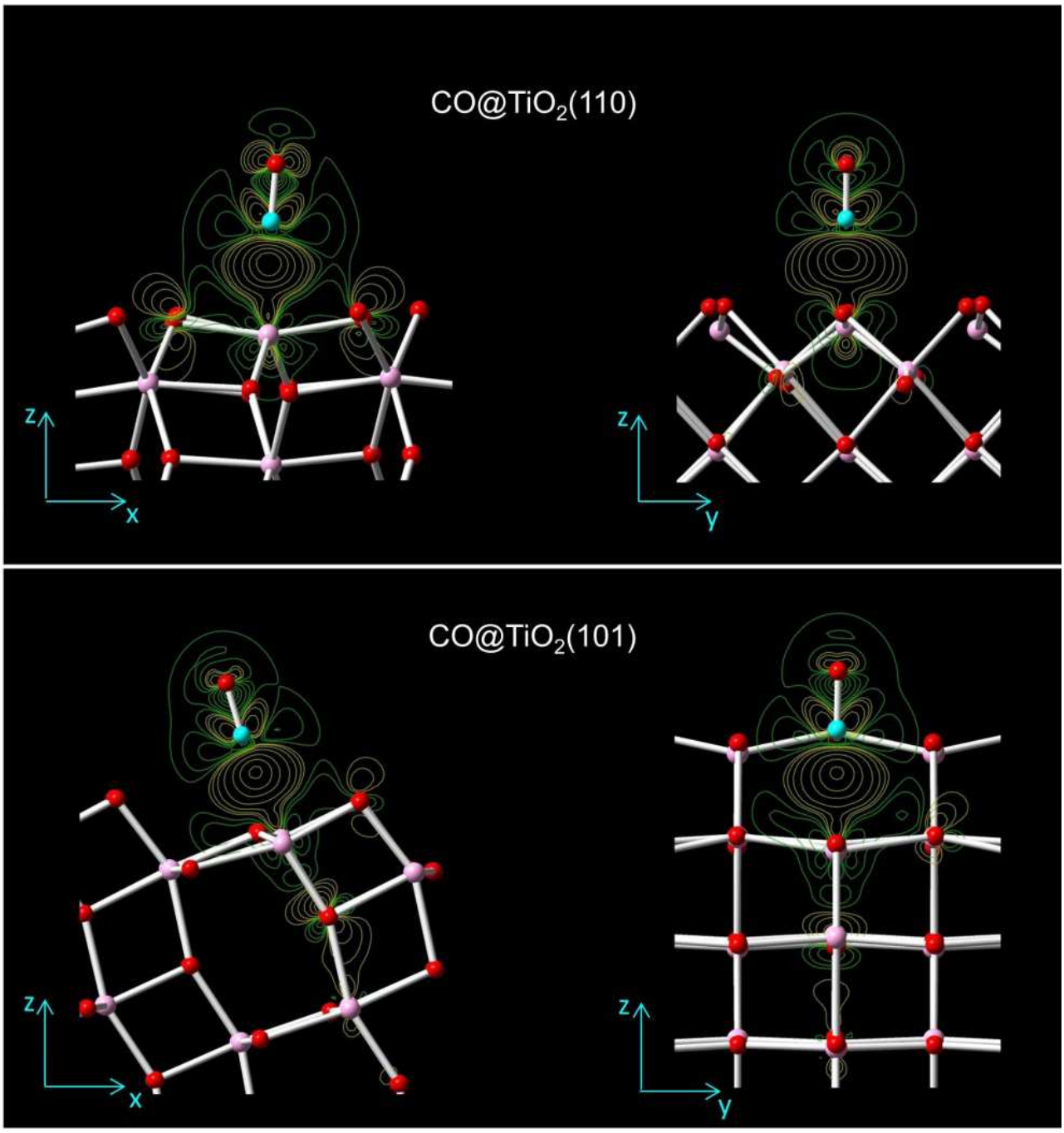

Figure S15. Bonding charge density contour plots on the xz (left) and yz (right) planes for the $CO@TiO_2(110)$ and $CO@TiO_2(101)$ systems. Yellow and green contour lines indicate charge accumulation and depletion regions, respectively. The Ti-C bond is not drawn for a better representation of contour lines between the C and Ti atoms. In all plots, the values of $\Delta\rho$ (in e/Å^3) associated to the contour lines are: 0.0005, 0.001, 0.002, 0.004, 0.008, 0.0012, 0.016 going from the outermost contour to the innermost one. For both systems, the 0.004 value here represented as a contour line, is also represented as isosurface in figure 4 of the main text. Atom colors: Ti=pink, O=red, C=cyan.

Reference

M. Farnesi Camellone, J. Zhao, L. Jin, Y. Wang, M. Muhler, D. Marx, *Angew. Chem. Int. Ed*. **2013**, *52*, 5780 5784; *Angew. Chem.* **2013**, *125*, 5892–5896.

2.2.3 Validation of the electronic structure calculations

In order to validate the electronic structure of the $CO@TiO_2(110)$ and $CO@TiO_2(101)$ systems, calculated with the PBE functional, single-point calculations with the hybrid density functional PBE0 (see the reference of this subsection) were performed on the optimized structures of both systems. Using the same geometry, single-point PBE0 calculations were also performed for the isolated $TiO_2(110)$ and $TiO_2(101)$ surfaces, as well as for the isolated CO molecule. The PBE0 single point calculations on the isolated subsystems (i.e. the surface and the CO molecule) were performed in order to obtain the PBE0-bonding charge density, which is compared with the PBE one in Figure S16.

The figure clearly highlights the good agreement among results obtained with the PBE (a pure-DFT functional) and PBE0 (a hybrid-DFT functional) approaches. Most importantly, the accumulation of electron density between the Ti and C atoms and the magnitude and shape of the charge accumulation region around the oxygen atom of CO calculated with PBE0 are very well reproduced by PBE. Minor differences are detected only in the region close to the carbon atom of CO in the case of $CO@TiO_2(110)$. This comparison therefore fully validates the conclusions based on the PBE electronic structural results.

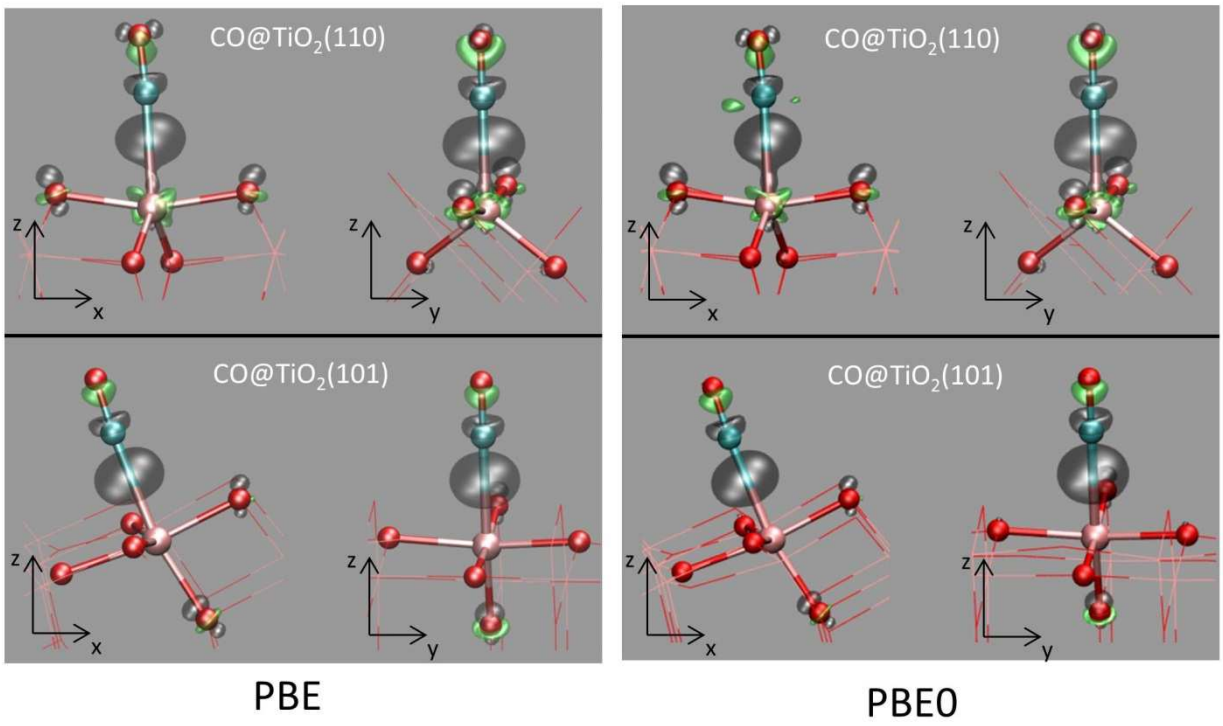

Figure S16. Bonding charge density isosurfaces calculated for the $CO@TiO_2(110)$ and $CO@TiO_2(101)$ systems with the PBE functional (left) and with the hybrid PBE0 functional (right). Charge accumulation regions = grey, depletion regions= green. The PBE bonding charge density (also depicted in Figure 4 in the main text) is shown in order to facilitate comparison between PBE and PBE0 results. Atom color and representation as in Figure 4 of the main text**.**

Reference

C. Adamo, V. Barone, *J. Phys. Chem.* **1999**, *110*, 6158-6169.